Journal of Renewable Materials

Tech Science Press

DOI: 10.32604/jrm.2021.014379

ARTICLE

Road Performance, Thermal Conductivity, and Temperature Distribution of Steel Slag Rubber Asphalt Surface Layer

Zhiqiang Shu, Jianmin Wu*, Shaoqing Li, Bingbing Zhang and Jianqi Yang

Key Laboratory of Special Area Highway Engineering of Ministry of Education, Chang'an University, Xi'an, 710064, China

*Corresponding Author: Jianmin Wu. Email: wujm@chd.edu.cn

Received: 22 September 2020 Accepted: 27 October 2020

ABSTRACT

The use of steel slag, which is a by-product of the steel manufacture, in the construction of asphalt pavement would contribute to waste reduction and environment protection. Using rubber asphalt at the same time can improve the performance of asphalt mixture. This study investigates the influence of steel slag content on the road performance, thermal conductivity and outdoor temperature distribution of steel slag rubber asphalt mixtures (SSRAM), and calculates the cumulative stress in surface layer. At a certain range of concentration, the steel slag additive improved the deformation resistance and low-temperature cracking resistance of the mixtures. The SSRAM with 40% steel slag content has the best deformation resistance while SSRAM with 60% steel slag content performed well in low-temperature cracking resistance. The thermal conductivity of the SSRAM with different steel slag content (0%, 20%, 40%, 60%, 80%, and 100%) was 1.994, 2.188, 2.239, 2.255, 2.288, and 2.295 W/(m·K), respectively. Measurements of the outdoor temperature distribution further confirmed that steel slag increased the thermal conductivity of the mixtures, thereby increasing the cumulative temperature difference between the top and bottom layers. The temperature stress and temperature-stress ratio of the SSRAM with 40% steel slag were 0.43 MPa and 0.24, while the SSRAM with 100% steel slag were 0.58 MPa and 0.36. The stress and stress ratio were much higher in the SSRAM with 100% steel slag than in the specimen with 40% steel slag. Accordingly, the maximum accumulated temperature stress aggrandized and caused early temperature cracks in the surface layer. The optimum content of steel slag was 40%.

KEYWORDS

Steel slag; rubber; thermal conductivity; temperature stress; asphalt mixture

1 Introduction

Steel slag is a by-product of the steel making process. Recycled steel slag is used in the construction industry and agriculture, but a large amount of steel slag becomes discarded on the ground, imposing huge pressures on environmental protection. Previous studies showed that steel slag applied as a coarse aggregate in road engineering can meet engineering needs. The proper content of steel slag would improve the indirect tensile strength [1], high-temperature performance [2], low-temperature fatigue life [3,4], and other performance parameters of the asphalt mixture. Liu et al. prepared steel slag/steel fiber composit asphalt mixtures and finding that steel fibers and steel slag can enhance the induction heating speed, heating homogeneity. Their results showed that adding steel slag and/or steel fibers improves the

water stability, particle loss resistance and fracture energy of asphalt mixtures [5]. The surface characteristics of weathered steel slag coarse aggregate (SSCA) and its effect process on the moisture stability of asphalt mixture were determined by Chenet et al. For the serious freeze-thaw damage environment, weathered SSCA or organic modified weathered SSCA was suggested to prepare asphalt mixture with SBS modified asphalt and some Portland cement [6]. However, the addition of steel slag will increase the thermal conductivity of asphalt mixture, decreasing its low temperature performance, especially the content of steel slag added is higher than optimum. There are few studies on this problem.

The application of another raw material, rubber powder, has become relatively mature in road engineering [7−9]. Wang et al. determined the fatigue cracking property of a crumb rubber-modified asphalt mixture in a semi-circular bending test. Statistics showed that the rubber powder additive improved the fatigue life of asphalt mixture [10]. Ding et al. investigated the performance of the recycled asphalt concrete with stable crumb rubber asphalt (SCRA) binder by wheel-tracking test, low-temperature bending beam test, immersion test and four-point bending beam test. Test results showed that the low-temperature performance of the SCRA recycled asphalt mixtures could be improved further while the other performance retained a high level at the same time [11]. Several related studies have shown that the use of rubber asphalt can improve the performance of asphalt mixture [12−14]. Therefore, the use of steel slag rubber asphalt mixtures (SSRAM) not only solves the problem of pavement material shortage, but also relieves environmental pressure.

The thermal parameters of steel slag differ from those of natural gravel. Jiao et al. measured the thermal conductivity of Marshall specimens using a parallel hot-wire, setting heating devices at the bottom of the surface layer. They determined that an asphalt mixture containing 6% steel slag was more thermally conductive than the conventional asphalt mixture [15]. The thermal conductivity of a mixture is usually measured by the ASTM C177 method (i.e., “Standard test method for steady-state heat flux measurements and thermal transmission properties by means of guarded hot plate apparatus”) [16,17]. The thermal conductivity of materials have been extensively reported, and prediction models of thermal conductivity have been derived through theoretical analysis [18−20]. However, asphalt mixture is a temperature-sensitive material. Its thermal conductivity varies in different temperature regions and its change curve is nonlinear. For such materials, the flat plate method provides more accurate measurements [21,22]. Therefore, to analyze the temperature and mechanical properties of SSRAM, the thermal conductivity and temperature distributions in the SSRAM surface layers were measured by the flat plate method in the present study.

The application of SSRAM as the surface layer of pavement has been rarely reported. Based on previous studies, this article discusses the temperature performance and temperature distribution of the SSRAM surface layer, and recommends improvements on the temperature fatigue life of SSRAM. This study is expected to provide research experiences for the application of steel slag and rubber powder in asphalt pavement.

2 Raw Materials and Preparation

2.1 Steel Slag

The steel slag in this experiment was sourced from Anfeng Steel Mill in Hebei Province, China. The slag had been naturally aged for over one year. The coarse and fine aggregates in the asphalt mixture were composed of basalt and limestone, respectively (the basalt with particle sizes of 9.5~13.2 and 4.75~9.5 were both replaced isometrically by steel slag). The steel slag volume replacement level (replacing basalt) was varied as 0, 20%, 40%, 60%, 80%, and 100%. The chemical compositions of the steel slags are given in Tab. 1. The appearance of steel slag is showed in Fig. 1.

Table 1: Chemical compositions of the steel slag specimens

Particle size (mm)	Compound content (%)												
	CaO	Fe_2O_3	SiO_2	MgO	Al_2O_3	P_2O_5	MnO	TiO_2	SO_3	Cr_2O_3	K_2O	V_2O_5	else
9.5–13.2	45.05	24.28	13.46	3.11	4.55	1.56	5.22	1.38	0.31	0.51	0.08	0.30	0.19
4.75–9.5	42.45	21.19	20.12	2.93	4.37	1.54	4.14	1.27	0.51	0.58	0.25	0.31	0.34

Figure 1: The appearance of steel slag

The basicity of the steel slag was calculated as

$$B = \frac{M(CaO)}{M(SiO_2) + M(P_2O_5)} \tag{1}$$

where B and M are the basicity and chemical composition of the steel slag, respectively.

Inserting the values of Tab. 1 into Eq. (1), the basicity of the 9.5–13.2-mm particles was determined as high (B = 3.0), whereas that of the 4.75–9.5-mm particles was medium (B = 1.96). The immersion expansion rate of the steel slag was computed as

$$\gamma = \frac{(d_{10} - d_0) \times 100}{120} \tag{2}$$

where d_{10} is the count of the dial indicator after 10 days of hot and cold cycling, and d_0 is the initial count of the dial indicator.

The test results are plotted in Fig. 2. From this plot, the immersion expansion ratio of the steel slag was determined as 0.85%. The slag meets the requirements of Steel Slag for Wearing Asphalt Pavement (GB/T 24765-2009).

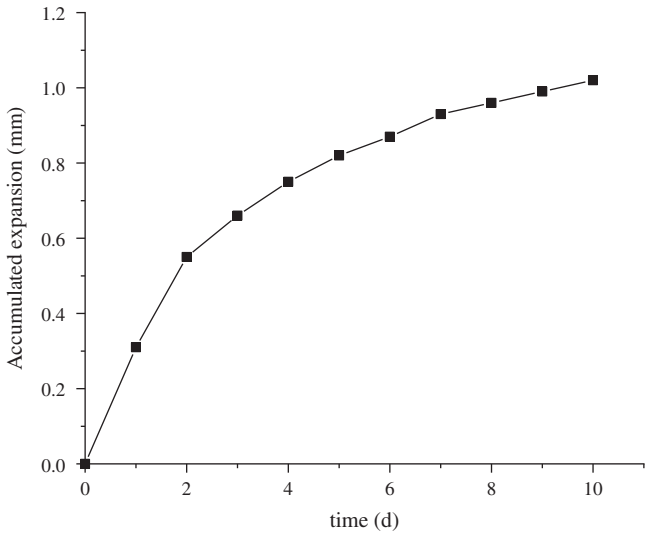

Figure 2: Accumulated expansion of steel slag over 10 days

2.2 Rubber Asphalt

Zhonghai A-70# asphalt was preheated to approximately 130°C, mixed with 18% 80-mesh rubber powder, and stirred evenly. The rubber asphalt was heated to 180°C, stirred by an impeller agitator for 1 h, and then stood for swelling at 170–180°C for 1 h. Tab. 2 gives the technical specifications of the rubber asphalt binder.

Table 2: Technical specifications of the rubber asphalt binder

Technical Index	Values	Text method
Penetration (25°C, 0.1 mm)	52	T 0604-2011
Penetration index PI	0.81	
Ductility (5 cm/min, 5°C, cm)	20	T 0605-2011
Softening point (°C)	62.4	T 0606-2011
Brookfield viscosity (Pa·s)	11.287 (165°C) 2.232 (180°C) 1.174 (190°C)	T 0625-2011
Elastic recovery (25°C)	78	T 0662-2011
Loss of weight (%)	0.206	T 0609 and T 0610-2011
Residual penetration ratio (25°C, %)	73.9	T 0604-2011
Residual ductility (10°C, cm)	21.4	T 0605-2011

2.3 Steel Slag Rubber Asphalt Mixtures

Tab. 3 gives the gradations of the SSRAM (here, the AC-13C gradation was adopted). From this table, the optimal asphalt-aggregation ratios of the mixtures with different steel slag contents were determined (SSRAM gradation design is based on volume-based specific gravity correction), the optimal asphalt-aggregation ratio determine method for SSRAM was Marshall compaction test, and the results are shown in Tab. 4.

Table 3: Gradations of SSRAM

Sieve size (mm)		16	13.2	9.5	4.75	2.36	1.18	0.6	0.3	0.15	0.075
Passing ratio (%)	Gradation	100	96	69	40	28	20	13	9	6	4
	Upper limit	100	100	85	68	50	38	28	20	15	8
	Lower limit	100	90	68	38	24	15	10	7	5	4

Table 4: Optimal asphalt-aggregation ratios of SSRAM

Content of steel slag	Gross volume density (g/cm^3)	VV (%)	VFA (%)	VMA (%)	Stability (kN)	Flow value (0.1 mm)	Asphalt-aggregation ratio (%)
0%	2.564	3.9	74.3	15.2	9.4	30	4.95
20%	2.582	3.9	74.8	15.5	9.6	28	5.15
40%	2.617	3.8	75.6	15.6	9.5	27	5.34
60%	2.633	3.9	75.3	15.8	9.5	29	5.48
80%	2.641	3.8	76.2	16.0	9.2	31	5.57
100%	2.646	3.8	76.4	16.1	9.1	33	5.65

3 Experimental Plan

3.1 Rutting Test

Following the standard test method T 0719-2011, the test temperature, wheel pressure, and wheel travel speed were set to 60°C, 0.7 MPa and 42 times/min, respectively. The specimen size was 300 mm × 300 mm × 50 mm.

3.2 Low-Temperature Bending Test

Following the standard test method T 0715-2011, the specimens were cut to size 250 mm × 35 mm × 30 mm, and tested in a universal testing machine. The test temperature and loading rate were −10°C and 50 mm/min, respectively.

3.3 Determination of Thermal Parameters of SSRAM

In this section, the thermal conductivity of the asphalt mixture was conveniently measured by the flat-wall heat conduction method [21,22]. The thermal parameters of the asphalt mixture were measured by a process with similarities to single flat-wall heat transfer, whose principle is shown in Fig. 3.

Assume that the cross-sectional area of the flat wall is S, the sides and upper surface are insulated, and the temperatures at the left and right sides of the flat wall are T_1, and T_2, respectively. Let δ, Φ_{in}, and Φ_{out} represent the thickness, input heat, and output heat of the specimen respectively.

The thermal conductivity and thermal diffusivity are respectively solved as $\lambda = \dfrac{\Phi\delta}{S\Delta T}$ and $K = \dfrac{\lambda}{c\rho}$.

3.4 Temperature Measurements and Temperature Stress Calculation of SSRAM

The temperature fields of asphalt pavements have been extensively reported [23,24]. This section determines the temperature distribution law of the SSRAM surface layer. First, a temperature sensor was placed on an outdoor AC-16 upper-surface layer and a spread tack coat. Second, the SSRAM surface layers with different steel slag contents were placed on the AC-16 layer, and temperature sensors were positioned on its upper surface. Third, the temperature sensors were connected to a data collection device,

and the temperature data were continuously collected for 45 days during the low-temperature season in Xi'an. Finally, the data of the collection device were derived and processed to calculate the temperature stress in the SSRAM surface layer.

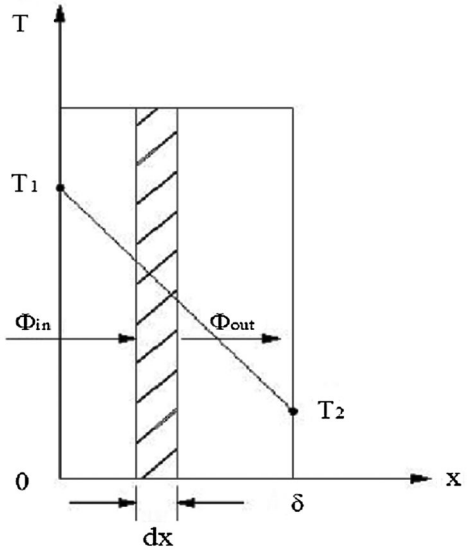

Figure 3: Schematic of flat-wall heat transfer

Hills et al. [25] researched the low-temperature shrinkage of asphalt pavement under the following assumptions:

An infinitely long asphalt pavement is blocked from shrinkage in the longitudinal direction, but can freely shrink in the transverse direction.

The asphalt mixture is a homogeneous and isotropic viscoelastic material.

Regardless of how the shrinkage affects the base course on the surface layer, the temperature stress of the asphalt mixture was assumed to be caused only by the shrinkage of the asphalt mixture. The calculation formula is

$$\sigma(t) = \alpha \sum_{T_0}^{T_1} S(t, T)\Delta T, \tag{3}$$

where $\sigma(t)$ is the cumulative temperature stress (MPa), T_0 and T_1 are the initial and final temperatures (°C), respectively, and ΔT is the temperature difference (°C). α is the temperature shrinkage coefficient ($°C^{-1}$), and $S(t, T)$ is the stiffness modulus of asphalt mixture (MPa).

4 Results and Discussion

4.1 High-Temperature Performance Analysis of SSRAM

Tab. 5 presents the dynamic stabilities of the SSRAM specimens with different steel slag contents. The dynamic stabilities of all specimens met the specification requirement. Obviously, the dynamic stability peaked when the steel slag content was 40%. At steel slag contents above 40%, the dynamic stability began to decrease. Steel slag has better angularity and reduces the flow of asphalt mixture under high temperature conditions of SSRAM. However, when the steel slag content increases, the optimal oil-stone ratio increases, and the main factor affecting the high temperature performance of SSRAM should be the

content of rubber asphalt. As evidenced in Fig. 4, increasing the steel slag content gradually increased the final rutting depth. When steel slag is incorporated into pavement, the allowable permanent deformation of the road must be considered.

Table 5: Dynamic stabilities of the SSRAM specimens

Content of steel slag	Rutting Depth (mm)		Dynamic Stability	Requirement (JTG F40-2004)	Construction requirements
	45 (min)	60 (min)			
0%	1.885	1.988	6117	≥2800	≥5000
20%	1.969	2.061	6848		
40%	2.23	2.321	6923		
60%	2.627	2.728	6238		
80%	2.967	3.076	5780		
100%	2.849	2.969	5250		

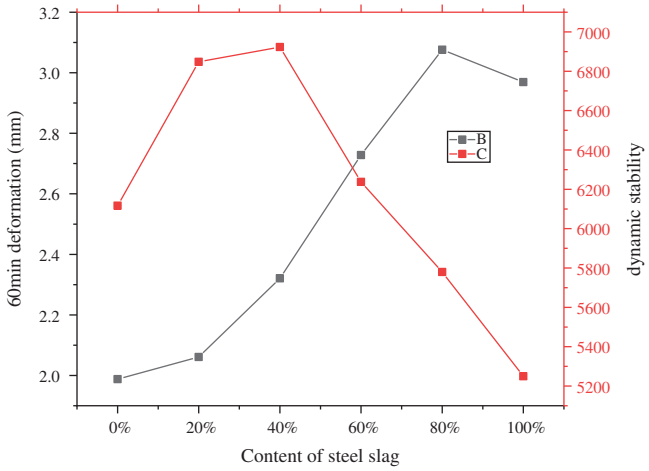

Figure 4: Comparison of rutting test results

4.2 Low-Temperature Performance Analysis of SSRAM

Under the same condition of asphalt mixture structure, SSRAM with different steel slag content corresponds to different optimal oil-stone ratio. Both the coarse aggregate and the asphalt-aggregation ratio in SSRAM have changed, and the low-temperature failure strain of SSRAM has changed significantly. In terms of their low-temperature failure strains (Tab. 6), the SSRAM specimens were ranked as follows: 60% > 40% > 80% > 20% > 0% > 100%. The failure strain of the SSRAM with 60% steel slag content was 8.19% higher than that of pure asphalt (0% SSRAM). Meanwhile, the flexural tensile strengths of the SSRAMs were ranked as 40% > 20% > 60% > 80% > 0% > 100%. The flexural tensile strength was 8.06% higher in the SSRAM with 40% steel slag than in the asphalt without steel slag. However, the low-temperature failure strain and flexural tensile strength were reduced in the SSRAM with 100% steel slag replacement. These results demonstrated that when incorporated at the optimal level, the steel slag improved the performance of the mixture.

Table 6: Low-temperature performance of SSRAM

Content of steel slag	Asphalt-aggregation ratio (%)	Failure strain (μ_ε)	Flexural tensile strength (Mpa)	Stiffness modulus (Mpa)
0%	4.94	2914.79	7.82	2685.54
20%	5.15	3044.75	8.41	2783.73
40%	5.34	3101.71	8.45	2729.04
60%	5.48	3153.64	8.37	2668.43
80%	5.57	3086.09	7.95	2598.43
100%	5.65	2862.13	7.22	2549.37

Steel slag is a porous material. From the perspective of structural asphalt and free asphalt, compared with basalt of the same particle size, steel slag has a larger specific surface area, so the steel slag has a stronger interaction with the surrounding asphalt. Steel slag will absorb more asphalt on the surface of the steel slag and form a layer of diffusion structure membrane with greater cohesion. When SSRAM is under stress, structural asphalt can provide stronger cohesion, thereby improving flexural tensile strength. However, once the content of steel slag exceeds the critical value, the content of free asphalt in the mixture begins to increase, which will lead to the decrease of failure strain, flexural tensile strength and stiffness modulus.

4.3 Thermal Conductivity Analysis of SSRAM

Fig. 5 shows the equipment of the thermal conductivity measurements. The upper and lower plates are the cooling and heating plates, respectively. The cooling plate has an internal water-circulation system that maintains a constant temperature. When heated to the target temperature, the heating plate provides a stable heating power that also maintains a constant temperature. The temperatures of the upper and lower plates were stabilized after 4–5 hours; at this time, the temperature difference, heating power, and specimen thickness were recorded. The thermal conductivity of the SSRAM specimens were calculated.

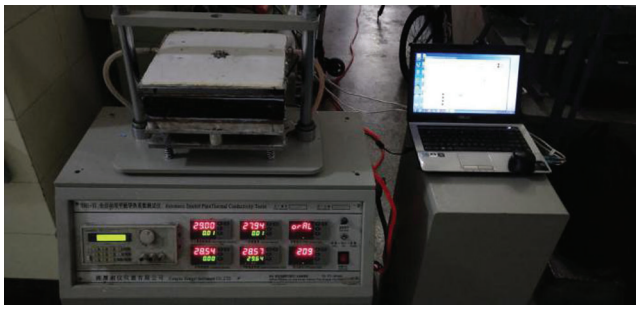

Figure 5: Equipment of the thermal conductivity tests

Tab. 7 shows the thermal conductivity of the SSRAM specimens with different steel slag contents. The steel slag additive increased the thermal conductivity of the mixtures. A steel slag content of 20% abruptly changed the thermal conductivity of the mixture. As the steel slag content increased further, the thermal conductivity steadily increased as shown in Fig. 6. According to the previous test results, SSRAM specimens with different steel slag contents have different optimal asphalt-aggregation ratios. Therefore, the factors affecting the thermal conductivity of SSRAM require further investigation.

Table 7: Thermal conductivity of the SSRAM specimens

Content of steel slag	Temperature difference (°C)	Heating power (W)	Specimen thickness (mm)	Thermal Conductivity (W/[m·K])
0%	16.00	5.72	50.2	1.994
20%	15.96	6.08	51.7	2.188
40%	15.77	6.28	50.6	2.239
60%	15.52	6.35	49.6	2.255
80%	15.92	6.39	51.3	2.288
100%	15.72	6.43	50.5	2.295

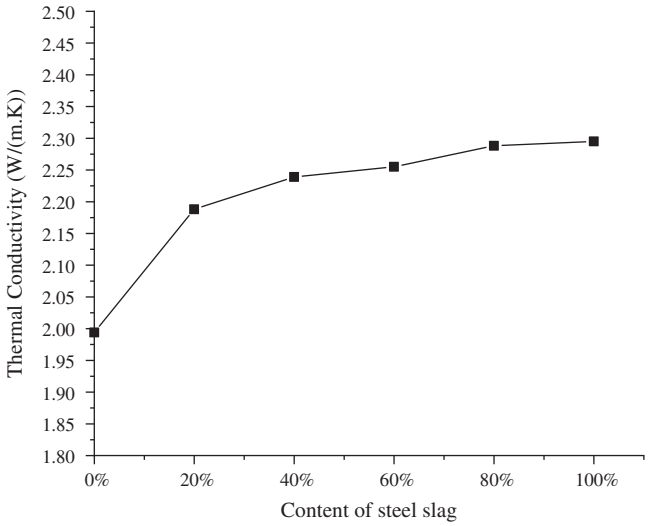

Figure 6: Thermal conductivity versus steel slag content in asphalt

4.4 Analysis of Temperature Distribution

4.4.1 Temperature Distribution in the SSRAM Surface Layer

The pavement structure is presented in Fig. 7. Fig. 8 shows the appearances of the SSRAM specimens with different contents of steel slag. The pavement temperature data were measured for 45 consecutive days in the low-temperature season in Xi'an.

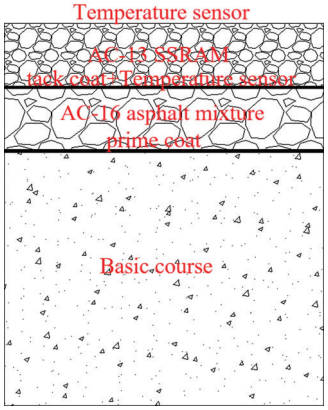

Figure 7: Schematic of the pavement structure

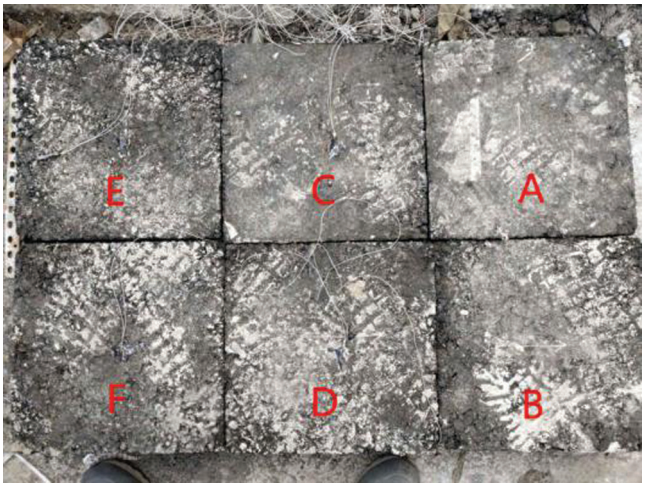

Figure 8: SSRAM specimens with different contents of steel slag placed outdoors for temperature measurements: (A) 0%, (B) 20%, (C) 40%, (D) 60%, (E) 80%, (F) 100%

The temperature data over three consecutive days are shown in Fig. 9. On all three days, the temperature of the pavement structure was lowest around 5:00–7:00 am and highest around 1:00–3:00 pm. Relative to the upper-surface temperatures, the highest and lowest temperatures at the bottom of the SSRAM surface layer were delayed by approximately one hour.

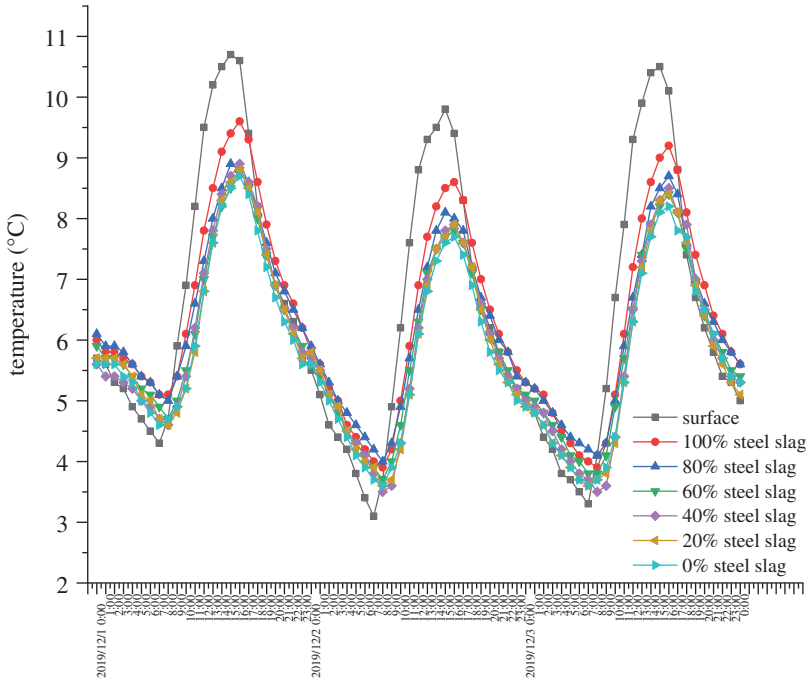

Figure 9: Temperature changes at the upper and lower surfaces of SSRAM pavement over three consecutive days ("Surface" represents the upper-surface layer, "0–100% steel slag" represents the lower-surface layer)

The temperature curves over 45 days are displayed in Fig. 10. The SSRAM specimens with different steel slag contents showed significant temperature differences between their upper and lower surface

layers. At the highest temperature on each day (Fig. 10a), the temperature difference between the upper and lower SSRAM layers was positive when the temperature increased, and the temperature stress on the bottom surface was compressive stress. At the lowest temperature on each day (Fig. 10b), the temperature difference was negative when the temperature decreased, and the temperature stress on the bottom surface was tensile stress. The temperature difference between the upper and bottom of the SSRAM layer gradually decreased with increasing content of steel slag, indicating that the steel slag affected the thermal conductivity. The steel slag additive decreased the absolute value of the temperature difference. Because a higher thermal conductivity indicates faster heat transfer, SSRAM can play a positive role in the melting of snow. In particular, the electrical–thermal at the bottom surface layer was superior to that of an ordinary asphalt mixture [12].

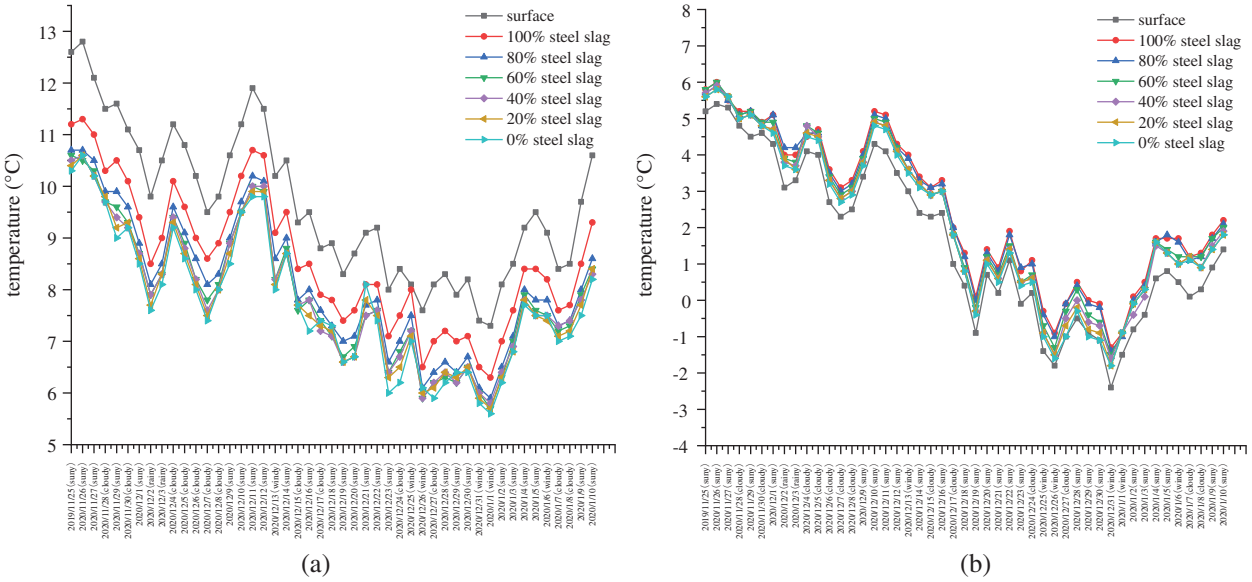

Figure 10: Temperature changes at the upper ("Surface") and lower ("0–100% steel slag") surfaces of the SSRAM pavements over 45 days: (a) Highest daily temperature and (b) Lowest daily temperature

Fig. 11 shows the temperature differences between the upper and lower surfaces of the SSRAM specimens, and Fig. 12 shows the averages and squared errors of the best-fitting curves to the temperature differences. At the lowest daily temperatures, the temperature difference linearly decreased with increasing steel slag content. The linear fits were strong with small data fluctuations. In contrast, the highest daily temperatures were nonlinearly related to steel slag content, and the data fluctuated more dramatically. This result can be explained by the temperature-sensitivity of asphalt concrete, meaning that its physical properties are closely related to temperature. Temperature changes are known to significantly affect the thermal conductivity of asphalt concrete [26].

During the temperature cycles, the maximum cumulative temperature at the bottom layer increased with increasing steel slag content, and the maximum accumulated temperature stress aggrandized accordingly.

4.4.2 Analysis of Temperature Stress

The temperature stress at the SSRAM surface layer was analyzed under the following assumptions based on Hills and Brien's theory:

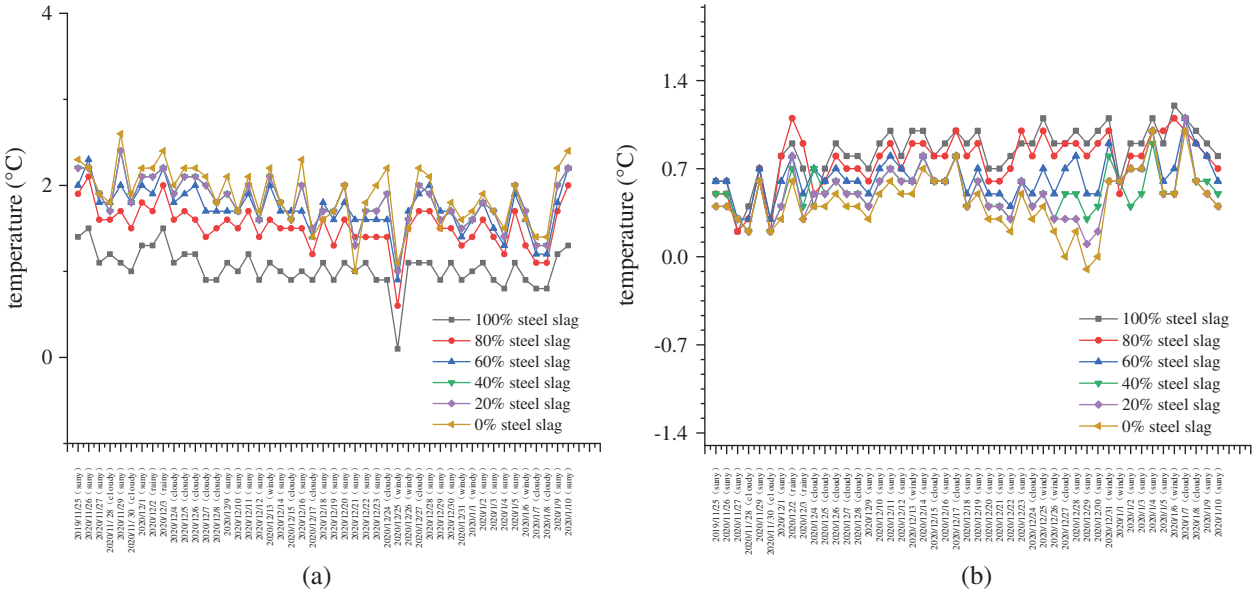

Figure 11: Temperature differences between the top and bottom SSRAM surfaces: (a) Highest daily temperatures and (b) Lowest daily temperatures

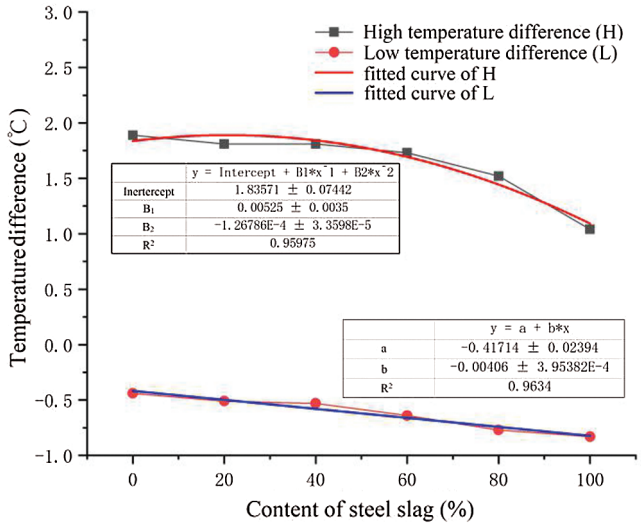

Figure 12: Fitted curves (average and square error) of the temperature difference between the top and bottom surface versus stag steel content

1. The temperature shrinkage coefficient, stiffness modulus, and tensile strength of SSRAM are constants over the temperature range of this study.
2. The expansion and contraction of the asphalt mixture are linearly related to the temperature difference:

$$\Delta\varepsilon = \alpha(T)\Delta T \tag{4}$$

$$\Delta W = \sigma(t)\Delta\varepsilon = \alpha^2(T)\Delta T \sum_{T_0}^{T_1} S(t,T)\Delta T \tag{5}$$

Under these assumptions, Eqs. (3)–(5) can be expressed as Eqs. (6)–(8), respectively:

$$\sigma = \alpha \sum_{T_0}^{T_1} S\Delta T \tag{6}$$

$$\Delta\varepsilon = \alpha\Delta T \tag{7}$$

$$\Delta W = \sigma\Delta\varepsilon = \alpha^2\Delta T \sum_{T_0}^{T_1} S\Delta T \tag{8}$$

$$N = k\left(\frac{1}{\sigma/\sigma_{\max}}\right)^n \tag{9}$$

where $\Delta\varepsilon$ is the strain in the SSRAM caused by a small instantaneous temperature difference, α is the temperature shrinkage coefficient, ΔW is the instantaneous strain energy, N is the temperature fatigue life (given by Eq. (9)), and k and n are coefficients determined by the physical properties of SSRAM.

Eq. (6) estimates the temperature stress at the bottom of the SSRAM surface layer, and Eq. (7) estimates the instantaneous strain energy under the temperature stress. Note that the instantaneous strain energy is useful only for estimating instantaneous temperature gradients, because the periodic temperature change is equivalent to applying a periodic strain on the SSRAM. Therefore, it produces a stress response after the strain acts, and the strain energy then dissipates [27,28]. Eq. (9) is the fundamental formula of fatigue life. Clearly, the fatigue life of an asphalt mixture is strongly affected by the stress ratio.

The calculated parameters of temperature stress are shown in Tab. 8. The maximum accumulated temperature stress and temperature-stress ratio at the surface were calculated by Eq. (6).

Table 8: Calculated parameters of temperature stress

Content of steel slag	α(1×10^{-5}/°C)	S(Mpa)	Indirect tensile strength (Mpa, −10°C)
0%	2.16	2685.54	1.619
20%	2.475	2783.73	1.738
40%	2.79	2729.04	1.791
60%	3.105	2668.43	1.762
80%	3.42	2598.43	1.716
100%	3.735	2549.37	1.637

Considering the influence of the steel slag expansion on temperature stress, Fig. 13 plots the maximum cumulative temperature stresses and stress ratios on consecutive days. The maximum cumulative temperature stress at the bottom of the SSRAM surface increased after adding the steel slag. In the specimens with steel slag contents of 0%, 20%, 40%, 60%, 80%, and 100%, the average temperature stresses at the surface layer after 45 days were 0.33, 0.39, 0.43, 0.47, 0.51, and 0.58 MPa, respectively, and the temperature-stress ratios were 0.20, 0.23, 0.24, 0.26, 0.30, 0.36, respectively. The temperature stress and temperature-stress ratio were 0.1 MPa and 0.04 higher, respectively, in the SSRAM with 40% steel slag than in the asphalt mixture without steel slag. In the SSRAM specimen with 100% steel slag, the temperature stress and its ratio were 0.25 MPa and 0.16 higher, respectively, than in the pure asphalt specimen. Obviously, the stress and stress ratio were much higher in the SSRAM with 100% steel slag than in the SSRAM with 40% steel slag.

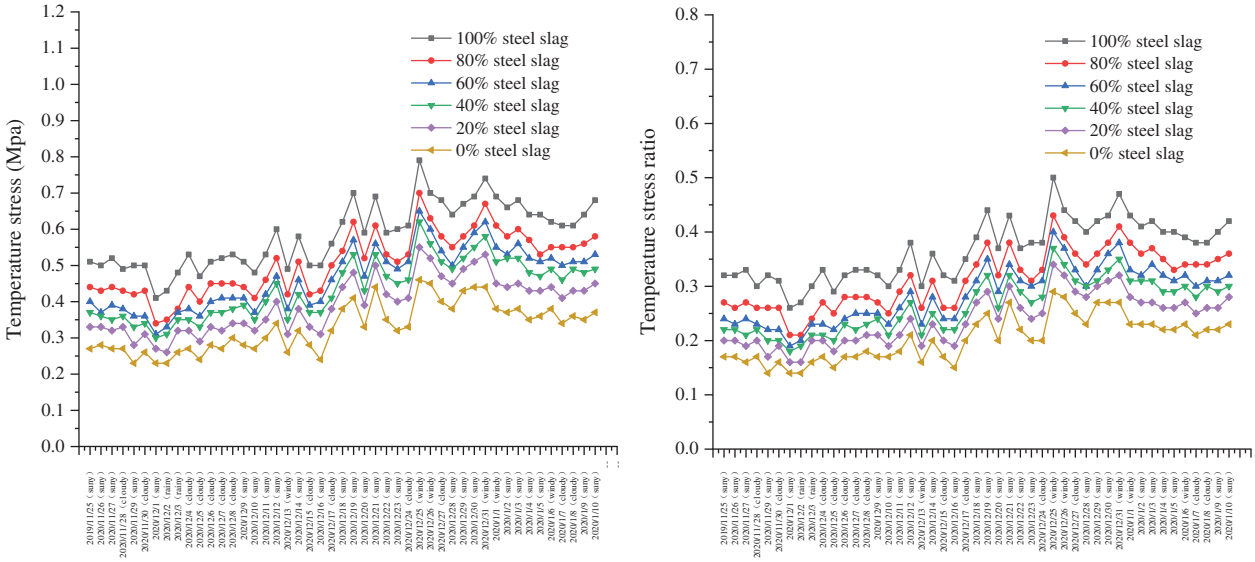

Figure 13: Maximum cumulative temperature stresses (a) and temperature-stress ratios (b) in the SSRAM specimens on successive days

By Eq. (8), the instantaneous strain energy at the SSRAM surface was related to the steel slag content and the physical characteristics of the steel slag. Therefore, selecting steel slag with a low immersion expansion ratio can reduce the instantaneous strain energy. After determining the physical parameters k and n of the mixtures in the test, the fatigue life of the SSRAM can be calculated by Eq. (9).

In engineering applications, using steel slag with a low immersion expansion rate can reduce the temperature shrinkage rate and maximum cumulative temperature stress of the SSRAM. Alternatively, adding fibers can enhance the tensile strength of the SSRAM surface layer, thereby reducing the temperature-stress ratio and improving the fatigue life of the surface layer.

The above analyses confirm the importance of adding an appropriate steel slag content to SSRAM. Excessive steel slag content will raise the temperature stress and stress ratio, causing early temperature cracks in the surface layer. The content of steel slag should not greatly affect the temperature stress and fatigue life of the SSRAM; accordingly, the proper steel slag content was determined as 40%.

5 Conclusions

Rutting tests and low-temperature bending tests were carried out on SSRAM specimens with different steel slag contents. The thermal conductivity of the SSRAM surface layers were measured, and the temperature distributions of the lower SSRAM surfaces were analyzed by outdoors and indoors methods. The main conclusions from these results are outlined below:

1. SSRAM specimens were prepared with different contents of steel slag with an immersion expansion ratio of 0.85%, and the optimal asphalt-aggregation ratio was determined. A rutting test and a low-temperature bending test confirmed that the SSRAMs met the specification requirements. The SSRAM with 40% steel slag content has the best deformation resistance while SSRAM with 60% steel slag content performed well in low-temperature cracking resistance.
2. The thermal conductivity of the SSRAM with different steel slag content (0%, 20%, 40%, 60%, 80%, and 100%) were 1.994, 2.188, 2.239, 2.255, 2.288, and 2.295 W/(m·K), respectively. The thermal

conductivity of the mixture distinctly changed between 0% and 20% steel slag content, and increased steadily at higher steel slag contents.

3. The temperature stress and temperature-stress ratio of the SSRAM with 40% steel slag were 0.43 MPa and 0.24, while the SSRAM with 100% steel slag were 0.58 MPa and 0.36. The stress and stress ratio were much higher in the SSRAM with 100% steel slag than in the specimen with 40% steel slag. Considering the deformation resistance and low-temperature cracking resistance of SSRAM, the proper steel slag content was determined as 40%.
4. In engineering applications, using steel slag with a low immersion expansion rate can reduce both the temperature shrinkage rate of the SSRAM and its maximum cumulative temperature stress. Adding fibers can also enhance the tensile strength of the SSRAM surface layer, thereby reducing the temperature-stress ratio and improving the fatigue life of the surface layer. However, the low-temperature fatigue life of SSRAM must be investigated in future research.

Funding Statement: This research was funded by the Department of Transportation of Hebei Province (Grant No. TH1-202019). In addition, the authors would like to thank the reviewers of this paper for their ever-present support and valuable advice.

Conflicts of Interest: The authors declare that they have no conflicts of interest to report regarding the present study.

References

1. Asi, I. M., Qasrawi, H. Y., Shalabi, F. I. (2007). Use of steel slag aggregate in asphalt concrete mixes. *Canadian Journal of Civil Engineering, 34(8),* 902–911. DOI 10.1139/l07-025.
2. Maslehuddin, M., Sharif, A. M., Shameem, M., Ibrahim, M., Barry, M. S. (2003). Comparison of properties of steel slag and crushed limestone aggregate concretes. *Construction and Building Materials, 17(2),* 105–112. DOI 10.1016/S0950-0618(02)00095-8.
3. Ahmedzade, P., Sengoz, B. (2009). Evaluation of steel slag coarse aggregate in hot mix asphalt concrete. *Journal of Hazardous Materials, 165(1–3),* 300–305. DOI 10.1016/j.jhazmat.2008.09.105.
4. Pasetto, M., Baldo, N. (2012). Fatigue behavior characterization of bituminous mixtures made with reclaimed asphalt pavement and steel slag. *Procedia Social Behavioral Sciences, 53,* 297–306. DOI 10.1016/j.sbspro.2012.09.882.
5. Quantao, L., Bin, L., Erik, S. (2017). Research on the mechanical, thermal, induction heating and healing properties of steel slag/steel fibers composite asphalt mixture. *Applied Sciences, 7(10),* 1088. DOI 10.3390/app7101088.
6. Chen, Z. W., Gong, Z. L., Jiao, Y. Y., Wang, Y., Shi, K. et al. (2020). Moisture stability improvement of asphalt mixture considering the surface characteristics of steel slag coarse aggregate. *Construction and Building Materials, 251*. DOI 10.1016/j.conbuildmat.2020.118987.
7. Siddique, R., Naik, T. R. (2004). Properties of concrete containing scrap−tire rubber—An overview. *Waste Management, 24(6),* 563–569. DOI 10.1016/j.wasman.2004.01.006.
8. Yildirim, Y. (2007). Polymer modified asphalt binders. *Construction and Building Materials, 21(1),* 66–72. DOI 10.1016/j.conbuildmat.2005.07.007.
9. Mull, M. A., Stuart, K., Yehia, A. A. (2002). Fracture resistance characterization of chemically modified crumb rubber asphalt pavement. *Journal of Materials Science, 37(3),* 557–566. DOI 10.1023/A:1013721708572.
10. Wang, H., Dang, Z., Li, L., You, Z. (2013). Analysis on fatigue crack growth laws for crumb rubber modified (CRM) asphalt mixture. *Construction and Building Materials, 47,* 1342–1349. DOI 10.1016/j.conbuildmat.2013.06.014.
11. Ding, X., Chen, L., Ma, T., Ma, H. Gu, L. et al. (2019). Laboratory investigation of the recycled asphalt concrete with stable crumb rubber asphalt binder. *Construction and Building Materials, 203,* 552–557. DOI 10.1016/j.conbuildmat.2019.01.114.

12. Xie, J., Chen, J., Wu, S., Lin, J., Wei, W. (2013). Performance characteristics of asphalt mixture with basic oxygen furnace slag. *Construction and Building Materials, 38,* 796–803. DOI 10.1016/j.conbuildmat.2012.09.056.
13. Cosme, R. L., Emi, S. L. T. J., Calmon, J. L. (2016). Use of frequency sweep and MSCR tests to characterize asphalt mastics containing ornamental stone residues and LD steel slag. *Construction and Building Materials, 122,* 556–566. DOI 10.1016/j.conbuildmat.2016.06.126.
14. Cheng, Y., Chai, C., Liang, C., Chen, Y. (2019). Mechanical performance of warm−mixed porous asphalt mixture with steel slag and crumb−rubber-SBS modified bitumen for seasonal frozen regions. *Materials, 12(6),* 857. DOI 10.3390/ma12060857.
15. Jiao, W., Sha, A., Liu, Z., Jiang, W., Hu, L. et al. (2020). Utilization of steel slags to produce thermal conductive asphalt concretes for snow melting pavements. *Journal of Cleaner Production, 261,* 121197. DOI 10.1016/j.jclepro.2020.121197.
16. Xiao, J. Z., Song, Z. W., Zhang, F. (2010). An experimental study on thermal conductivity of concrete. *Journal of Building Materials, 13,* 17–21.
17. ASTM (2004). Standard test method for steady−state heat flux measurements and thermal transmission properties by means of the guarded−hot−plate apparatus. *ASTM C177,* West Conshohocken, PA: ASTM.
18. Wu, J., Hameury, J., Failleau, G., Blahut, A., Hammerschmidt, U. (2018). Design guideline for new generation of high−temperature guarded hot plate. *International Journal of Thermophysics, 39(2),* 540. DOI 10.1007/s10765-017-2344-1.
19. Zarr, R. R., Flynn, D. R., Hettenhouser, J. W., Brandenburg, N. J., Healy, W. M. (2016). Fabrication of a guarded −hot−plate apparatus for use over an extended temperature range and in a controlled gas atmosphere. In: Dinwiddie, R. B., White, M. A., McElroy, D. L. (eds.), *Thermal conductivity 28: Thermal expansion 16*. vol. *28*. Gaithersburg, MD: NIST, 235, 2006.
20. Wu, J., Morrell, R. (2012). Corrections for thermal expansion in thermal conductivity measurement of insulations using the high−temperature guarded hot−plate method. *International Journal of Thermophysics, 33(2),* 330–341. DOI 10.1007/s10765-011-1144-2.
21. Dubois, S., Lebeau, F. (2015). Design, construction and validation of a guarded hot plate apparatus for thermal conductivity measurement of high thickness crop−based specimens. *Materials and Structures, 48(1−2),* 407–421. DOI 10.1617/s11527-013-0192-4.
22. Yang, I., Kim, D., Lee, S. (2018). Construction and preliminary testing of a guarded hot plate apparatus for thermal conductivity measurements at high temperatures. *International Journal of Heat and Mass Transfer, 122,* 1343–1352. DOI 10.1016/j.ijheatmasstransfer.2018.02.072.
23. Yan, Z. (1984). Analysis of the temperature field in layered pavement system. *Journal of Tongji University, 3,* 76–84.
24. Kang, H. G., Zheng, Y. X., Cai, Y. C., Liu, Y. (2007). Regression analysis of actual measurement of temperature field distribution rules of asphalt pavement. *China Journal of Highway & Transport, 20(6),* 13–18.
25. Hills, J. F., Brien, D. (1966). The fracture of bitumens and asphalt mixes by temperature induced stresses. *Proceedings of the Association of Asphalt Paving Technologists, 35,* 292–309.
26. Gong, X., Romero, P., Dong, Z., Li, Y. (2017). Investigation on the low temperature property of asphalt fine aggregate matrix and asphalt mixture including the environmental factors. *Construction and Building Materials, 156,* 56–62. DOI 10.1016/j.conbuildmat.2017.08.142.
27. Guo, H., Li, Z. (2013). Structural damage identification method based on strain energy equivalence parameter. *Chinese Journal of Solid Mechanics, 34(3),* 286–291.
28. Gupta, R., Narayan, S. P. A. (2019). Tensile creep of asphalt concrete in repeated loading tests and its effect on energy dissipation. *International Journal of Pavement Engineering, 59(6),* 1–13. DOI 10.1080/10298436.2019.1654101.